Postfach 10 11 61
69451 Weinheim
Germany
Courier services:
Boschstraße 12
69469 Weinheim
Germany
Tel.: (+49) 6201 606 235
E-mail: solar-rrl@wiley.com

WILEY-VCH

Dear Author,

Please correct your galley proofs carefully and return them no more than four days after the page proofs have been received.

Please limit corrections to errors already in the text; cost incurred for any further changes or additions will be charged to the author, unless such changes have been agreed upon by the editor.

The editors reserve the right to publish your article without your corrections if the proofs do not arrive in time.

Note that the author is liable for damages arising from incorrect statements, including misprints.

Please note any queries that require your attention. These are indicated with a Q in the PDF and a question at the end of the document.

Reprints may be ordered by filling out the accompanying form.

Return the reprint order form by e-mail with the corrected proofs to Wiley-VCH: solar-rrl@wiley.com

To avoid commonly occurring errors, **please ensure that the following important items are correct** in your proofs (please note that once your article is published online, no further corrections can be made):

- **Names** of all authors present and spelled correctly
- **Addresses** and **postcodes** correct
- **E-mail address** of corresponding author correct (current email address)
- **Funding bodies** included and grant numbers accurate
- **Title** of article OK
- All **figures** included
- **Equations** correct (symbols and sub/superscripts)

Corrections should be made directly in the PDF file using the PDF annotation tools. If you have questions about this, please contact the editorial office. The corrected PDF and any accompanying files should be uploaded to the journal's Editorial Manager site.

WILEY-VCH

AUTHOR QUERY FORM

JOURNAL: SOLAR RRL

Article: solr.202200101

Dear Author,

During the copyediting of your manuscript the following queries arose.

Please refer to the query reference callout numbers in the page proofs and respond to each by marking the necessary comments using the PDF annotation tools.

Please remember illegible or unclear comments and corrections may delay publication.

Many thanks for your assistance.

Query No.	Query	Remark
Q-license	Please note that the article can only be published once an appropriate license agreement has been signed. The responsible corresponding author will have received an e-mail invitation to register/log in and sign a license agreement in Wiley Author Services (https://authorservices.wiley.com). The costs of publishing this manuscript OnlineOpen might be covered by one of Wiley's national agreements. To find out more please visit, https://authorservices.wiley.com/author-resources/Journal-Authors/open-access/affiliation-policies-payments/index.html. Eligibility for fee coverage is determined by the affiliation of the responsible corresponding author.	
Q1	Please shorten Table of Contents text to a maximum of 60 words. All abbreviations should be defined.	
Q2	Please confirm that forenames/given names (blue) and surnames/family names (vermilion) have been identified correctly.	
Q3	Please note that the abbreviation "D–A" has been defined as "donor–acceptor." Please check that the added expansion is correct.	
Q4	"P. R. China" and "China" both have been used in the author affiliations as the country name. Please use one of these consistently.	
Q5	Please provide expansion for the abbreviation "IDIC" and "DTT."	
Q6	Please provide expansion for the abbreviation " PTQ10:BTP-FTh."	
Q7	Please provide the expansion for acronym "TP-2-PIE" at its first occurrence in the text.	
Q8	Please note that footnotes are not permitted in Table headings. So, it has been inserted in the first column. Please check that this is OK or move to a more appropriate place.	
Q9	Figure labels "a–f" have been provided in the artwork for Figure 5 but are not cited in the text. Please add them to the text at an appropriate point.	
Q10	Please check all equations have been correctly typeset.	
Q11	Please provide the expansion for acronyms "PCBM" at their first occurrence in the text.	
Q12	Please provide expansion for the abbreviations "PEDOT" and "PSS."	
Q13	Display lists are not the preferred style, so run-on format for lists has been used. Please check that the changes made are correct.	
Q14	Please provide expansion for the abbreviation "AR."	
Q15	Please provide volume/page number in refs. [24], if available.	
Q16	Please check that the publisher location added in ref. [41] is correct.	

Author: Please confirm that Funding Information has been identified correctly.

Please confirm that the funding sponsor list below was correctly extracted from your article: that it includes all funders and that the text has been matched to the correct FundRef Registry organization names. If a name was not found in the FundRef registry, it may not be the canonical name form, it may be a program name rather than an organization name, or it may be an organization not yet included in FundRef Registry. If you know of another name form or a parent organization name for a "not found" item on this list below, please share that information.

FundRef Name	FundRef Organization Name
National Natural Science Foundation of China	National Natural Science Foundation of China

RESEARCH ARTICLES

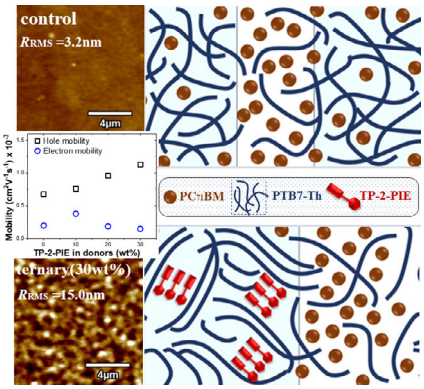

Using a discotic liquid crystal material (TP-2-PIE) having a self-organized property as a third component is able to alter Flory–Huggins molecular interaction parameters in donors and enhance phase separations (poly[4,8-bis(5-(2-ethylhexyl)thiophen-2-yl)benzo[1,2-b:4,5-b']dithiophene-co-3-fluorothieno [3,4-b]-thiophene-2-carboxylate] [PTB7-Th] with TP-2-PIE) and acceptor ([6,6]-phenyl-C_{71}-butyric acid methyl ester [$PC_{71}BM$]). This can tune the charge carrier mobility and density of defect states in the active layer and improve device performance.

Solar RRL
www.solar-rrl.com

Tuning Molecular Interaction in Polymer Solar Cells via a Multifunctional Discotic Component to Enhance Photovoltaic Response

Han Li, Hongkang Gong, Mengjie Sun, Huimin Zhang, Chao Ji, Chunjun Liang, Fangtian You, Xiping Jing, Xiangfei Kong,* and Zhiqun He*

A donor–acceptor (D–A)-type discotic organic material (TP-2-PIE) having a self-organization ability is selected to be the third component blending with poly[4,8-bis(5-(2-ethylhexyl)thiophen-2-yl)benzo[1,2-b:4,5-b']dithiophene-co-3-fluoro-thieno [3,4-b]-thiophene-2-carboxylate] (PTB7-Th): [6,6]-phenyl-C_{71}-butyric acid methyl ester ($PC_{71}BM$) in ternary bulk-heterojunction polymer solar cells. The complementary absorption and energy transfer between TP-2-PIE and PTB7-Th contributes to the enhancement in photocurrent generation, improving the short-circuit current. In addition, TP-2-PIE alters the molecular interaction leading to an enhanced phase separation, which promotes carrier transport with a good balance and minimizes the density of trap states simultaneously. In this way, the overall photovoltaic performances are markedly enhanced at an optimal condition of 10 wt% TP-2-PIE in donors with a 12.6% efficiency increase. Current understanding on the functionality of this third component in ternary solar cells may be able to guide future device development.

1. Introduction

Device engineering of polymer solar cells (PSCs) have made impressive progress in many aspects in recent years.[1–8] Techniques including synthesizing novel materials having better properties, matching optical absorption to maximize light harvesting, manipulating morphology of the active layer, and/or employing ternary blends for fine tune device performance.[9–12] Functional organic electronic or semiconducting materials are among the most promising classes being developed due to their advantages in low-cost fabrication, light weight, and potential flexibility. Organic electronic materials, in particular, those having liquid crystalline (LC) phases, play a crucial role in tuning photovoltaic device performance or exploring the device physics. Although rod-like, calamitic LCs have been substantially exploited in display applications, whereas disc-like or discotic LC (DLC) finds more interest in the field of organic optoelectronic applications. The DLC materials possess many advantages, such as their ease to self-organize into π–π-stacked columnar assemblies via strong molecular interactions; their charge carrier transport can be many orders of magnitude higher in a particular direction, for example, an excellent exciton diffusion length (≈70 nm) and a very high charge carrier mobility (≈1 $cm^2 V^{-1}s^{-1}$) in hexahexylthiotriphenylene[13] due to a much stronger intra-column molecular interaction than that of intercolumns.[13–15] In addition, DLCs display self-healing of structural defects owing to their LC nature.[16]

Coincidentally, the early organic solar cell with a power conversion efficiency (PCE) about 1% reported by Tang in 1986 was prepared by a heterojunction structure consisting of two discotic molecules, copper phthalocyanine, and perylene tetracarboxylic derivative.[17] The pioneer work carried out using a well-defined hexa-peri-hexabenzocoronene (HBC)-based DLC to prepare heterojunction photovoltaic device (PCE≈2%) in combination with perylene diimide was reported by Schmidt-Mende et al. in 2001.[18] DLC hexaacetoxytriphenylene has been effectively used as an additive at 3 wt% in P3HT:PC61BM–based bulk-heterojunction (BHJ) solar cells leading to an enhancement in PCE from 3.03% to 3.97%.[19] However, the early LC materials (either rod-like or discotic) have a limited optical absorption due to relative simple core structure. They are not ideal components to directly use either as a donor or as an acceptor. A breakthrough was made with a number of small molecules as a third component. In 2015, a highly crystallized small organic molecule (p-DTS-$(FBTTH_2)_2$ as a third component was found to induce a π–π stacking of poly[4,8-bis(5-(2-ethylhexyl)thiophen-2-yl)

H. Li, H. Gong, M. Sun, H. Zhang, C. Ji, C. Liang, F. You, Z. He
Key Laboratory of Luminescence and Optical Information
Ministry of Education
Institute of Optoelectronic Technology
Beijing Jiaotong University
Beijing 100044, P. R. China
E-mail: zhqhe@bjtu.edu.cn

X. Jing
College of Chemistry and Molecular Engineering
Peking University
Beijing 100871, P. R. China

X. Kong
College of Chemistry and Bioengineering
Guilin University of Technology
Guilin 541004, China
E-mail: xiangfei.kong@glut.edu.cn

The ORCID identification number(s) for the author(s) of this article can be found under https://doi.org/10.1002/solr.202200101.

DOI: 10.1002/solr.202200101

benzo[1,2-b:4,5-b']dithiophene-co-3-fluorothieno [3,4-b]-thiophene-2-carboxylate] (PTB7-Th) perpendicular to the substrate, with a face-on orientation, and achieved a PCE up to 10.5%.[20] Similarly, a nematic LC benzodithiophene terthiophene rhodanine (BTR) material was developed by Sun et al. in 2015, which has a broad enough optical absorption and is able to form highly oriented structures via solvent annealing. The photovoltaic device prepared with BTR as a donor and [6,6]-phenyl-C_{71}-butyric acid methyl ester ($PC_{71}BM$) as an acceptor achieved a PCE up to 9.3%.[21] Later, Ma et al. in 2017 employed BTR as a third component at 10 wt%, which raised the PCE of a PTB7-Th:$PC_{71}BM$–based device up to 10.83%.[22] Only 5 wt% of BTR as a third component was able to boost PCE of PM6:Y6–based device to 16.6%.[23] More recently, by introducing highly crystalline molecules (IDIC as a third component and DTT as an additive) into a novel PTQ10:BTP-FTh blend, a record high efficiency of 19.05% can be realized.[24]

With the progressive enhancement in PCE of BHJ PSCs, however, the low crystallinity of the donor polymer, the difficulty in donor/acceptor phase separation, as well as the weak light absorption in active layers leave a legacy of difficulty in PCE improvement.[25] By optimization of the active-layer morphology, as well as broadening of light absorption, the short–circuit density (J_{SC}) and fill factor (*FF*) of PSCs could be increased.[26–28] Solvent or small molecular additive in an active layer has been a common method, in addition to thermal annealing, to manipulate morphology or crystallinity of the active layers.[29,30] Liquid crystal components have been regarded as a very promising selection in tuning the morphology of the active layers, in particular, the phase separation of donor and accepter blends, thanks to its natural feature of self-assembly.[19,26,29]

In this work, a DLC TP-2-PIE[31] was selected as a third component in combination with PTB7-Th as a donor and $PC_{71}BM$ as an acceptor to fabricate PSCs. TP-2-PIE was particularly interesting as it has both electron donating and accepting units in the molecular structure. This investigation revealed that with the TP-2-PIE component, the photovoltaic performance of the devices was substantially enhanced. The functionalities of the TP-2-PIE component and physics of the device have been studied.

2. Results and Discussion

2.1. Polymer Photovoltaic Devices Tuning by a Discotic Liquid Crystal Component

A BHJ polymer photovoltaic cell was initially fabricated with an inverted configuration: ITO/ZnO/active layer/MoO_3/Ag as seen in **Figure 1**a, where the active layer consisted of a PTB7-Th polymer as a donor and fullerene $PC_{71}BM$ as an acceptor, which was blended at a weight ratio of 1:1.5. Their molecular structures are shown in **Figure 2**.

Current density–voltage (*J*–*V*) characteristics of the devices were measured under AM 1.5 irradiation at 100 mW cm^{-2} light intensity in ambient conditions as shown in **Figure 3**a and the photovoltaic parameters obtained are listed in **Table 1**. The device exhibits a moderate performance with a short–circuit current (J_{SC}) of 17.37 mA cm^{-2}, an open-circuit voltage (V_{OC}) of 0.81 V, and a *FF* of 63.1%. The PCE of the device is about 8.76%. This work is attempting to explore how to further improve the device performance.

In a BHJ PSC, the selection of organic materials can be a crucial step determining the basic level of photovoltaic performance attainable. Further improvement by matching the material properties and/or tuning device structure can be achieved. The J_{SC}, V_{OC}, and *FF* of the devices, for example, are closely dependent on the optical density for photo-harvesting, the energy level of the donor and acceptor materials that affects the driving force for exciton disassociation, and the morphology for charge carrier transport and extraction at the electrodes. Although some device parameters can be intrinsic to the materials used to a great extent, optimization of the device structure may also improve the device performance. A number of approaches can be employed to optimize the active layer or device structures. In this work, we consider a ternary strategy to tune the active layer to enhance photovoltaic performance. Therefore, a discotic liquid crystal compound, TP-2-PIE (see Figure 2), having both electron donor (D) and acceptor (A) units of a donor–acceptor (D–A) structure, has been evaluated for its suitability to use as a third component based on the following considerations: 1) light harvesting; 2) energy levels matching; 3) energy or charge transfer; and 4) self-organization.

Optical absorption spectra of the pristine and blended materials were measured as shown in Figure 3b. It was found that the TP-2-PIE specimen demonstrated a strong visible absorption with a multiple peak in the range of 430–550 nm, but the PTB7-Th specimen absorbed at a longer wavelength, in between 600 and 750 nm. That is, the two absorptions from TP-2-PIE and PTB7-Th are complementary well to each other. The addition of the TP-2-PIE component into the active layer could substantially enhance its absorption at short wavelength range (see Figure 3b). This would benefit the light harvesting in the active layer. Optical bandgap of the TP-2-PIE can be estimated through a Tauc Plot, which is 1.74 eV as seen Figure S1 in Supporting Information.

The energy levels of the TP-2-PIE, such as the highest occupied molecular orbital (HOMO) level and the lowest unoccupied molecular orbital (LUMO) level of TP-2-PIE, have been reported in previous work, to be −5.36 and −3.63 eV, respectively, measured by a cyclic voltammetry method.[31] An energy diagram including all functional layers is sketched in Figure 1b. It can be seen that the energy levels of TP-2-PIE match well with PTB7-Th. If PTB7-Th and $PC_{71}BM$ are used as donor and acceptor in the active layer, TP-2-PIE is expected to function as an extra donor according to its energy levels.

What is particularly interesting with the TP-2-PIE material is that this molecule has a triphenylene–perylene dyad structure linked through an ethynylphenyl bridge. However, the electron-donating (D) triphenylene moiety and the electron-accepting (A) perylene unit are decoupled in the TP-2-PIE dyad. According to the molecular simulations, the triphenylene moiety determines HOMO and the perylene monoimide diester unit governs the LUMO level of the TP-2-PIE dyad.[31] The D–A-type TP-2-PIE molecule does not respond to the light absorption and excitation as a whole. Instead, the two units are able to respond to the light individually as if they were independent molecules. Nevertheless, the D–A structure ensures the material has dual functionalities, either as a donor or as an acceptor depending on the counterpart species. The electron-rich conjugated bridge might promote intramolecular

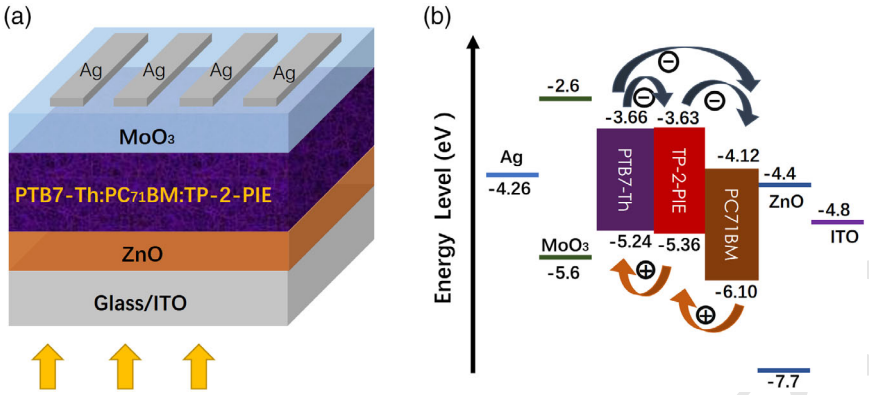

Figure 1. a) A schematic sketch of the device structure and b) an energy diagram of the device layers, where the values according to Kong et al. and Hofinger et al.[31,63,64] The carrier transport directions are indicated in arrows.

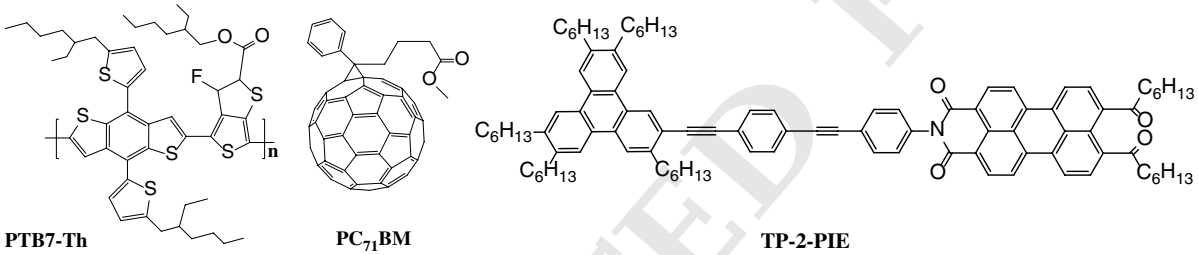

Figure 2. Chemical structures of poly[4,8-bis(5-(2-ethylhexyl)thiophen-2-yl)benzo[1,2-b:4,5-b']dithiophene-co-3-fluorothieno [3,4-b]-thiophene-2-carboxylate] (PTB7-Th), [6,6]-phenyl-C_{71}-butyric acid methyl ester ($PC_{71}BM$), and TP-2-PIE.

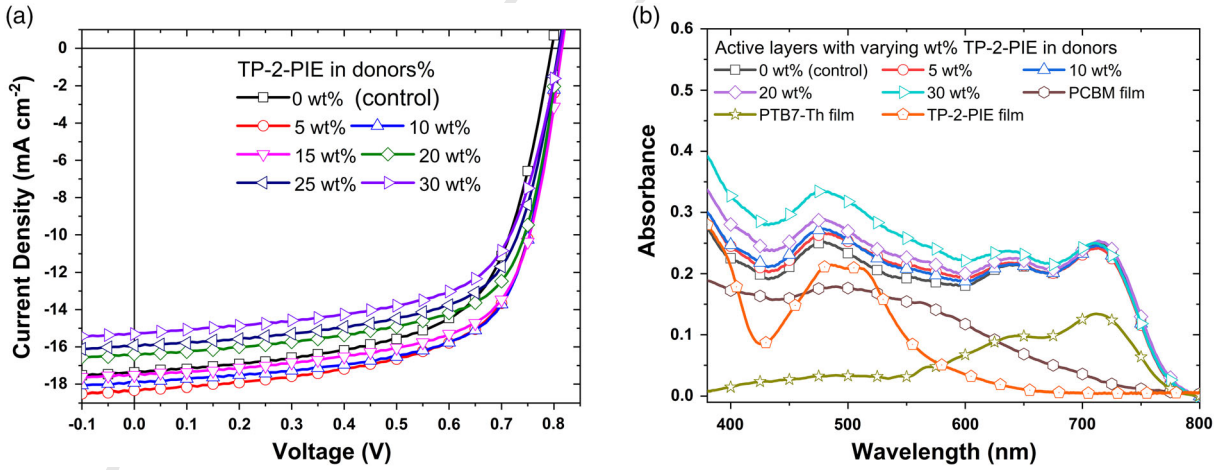

Figure 3. a) *J–V* characteristics measured under illumination of the devices, and b) UV-vis absorption spectra of the active layers and pristine specimens.

charge transfer within the molecular skeleton and promote charge-separated states of the molecules.[32]

In addition, the DLC TP-2-PIE has an advantage for molecular orientation. A homeotropic alignment is frequently a preferred orientation.[15,33,34] This has the potential to induce an ordered structure in the aggregate, which may be beneficial for the charge carrier transporting properties.[15,31,33]

Based on the earlier considerations, a series of ternary photovoltaic devices were fabricated using TP-2-PIE as the third component to mix with PTB7-Th to form a composite donor (PTB7-Th:TP-2-PIE). The active layers then become $PTB7\text{-}Th_{1-x}$:TP-2-PIE_x:$PC_{71}BM$, where the fraction × was taken from 0, 5, 10, 15, 20, 25, and 30 wt%, respectively. The total weight ratio between donors and acceptors was kept unchanged at 1:1.5.

J–V characteristics and the photovoltaic parameters of the devices were measured as given in Figure 3a and Table 1. About 20 cells were repeatedly fabricated and measured at each condition to ensure reproducibility. The statistical data can be found in Figure S2, Supporting Information. It is clear that the optimized device was the one with an active layer consisting

Table 1. Photovoltaic parameters derived from *J–V* measurements of devices with different weight ratio of TP-2-PIE in donors.

PTB7-Th:TP-2-PIE: $PC_{71}BM$ (weight ratio)[a)]	V_{OC} [V]	J_{SC} [mA cm^{-2}]	*FF* [%]	*PCE* [%]	R_S [Ω]	$R_{SH} \times 10^2$ [Ω]
1:0:1.5 (control)	0.81	17.37	63.1	8.76	6.23	4.84
0.95:0.05:1.5	0.81	18.32	66.1	9.80	5.82	6.32
0.90:0.10:1.5	0.81	17.92	68.0	9.86	5.71	6.97
0.85:0.15:1.5	0.81	17.53	66.9	9.61	4.79	6.77
0.80:0.20:1.5	0.81	16.39	67.1	8.90	4.92	6.78
0.75:0.25:1.5	0.81	15.92	65.9	8.50	5.91	6.41
0.70:0.30:1.5	0.81	15.32	64.7	8.02	6.66	5.80

[a)] PTB7-Th: poly[4,8-bis(5-(2-ethylhexyl)thiophen-2-yl)benzo[1,2-b:4,5-b']dithiophene-co-3-fluorothieno [3,4-b]-thiophene-2-carboxylate]; $PC_{71}BM$: [6,6]-phenyl-C_{71}-butyric acid methyl ester; FF: fill factor.

of PTB7-Th:TP-2-PIE:$PC_{71}BM$ at a ratio of 0.9:0.1:1.5, which achieved $V_{OC} = 0.81$ V, $J_{SC} = 17.92$ mA cm^{-2}, and $FF = 68\%$, along with a 12.5% increment in PCE in comparison with that from the control device. The best PCE in the ternary device approached 9.86%.

It is interesting to note that the addition of TP-2-PIE component has no influence on V_{OC}. The similarity in V_{OC} of the devices is consistent with the similarity in energy levels between the two donors.[35] However, the addition of TP-2-PIE component in the donor does have a strong impact on the J_{SC}, *FF*, as well as series and shunt resistances (R_S and R_{SH}) of the devices to some extent (see Table 1). A small fraction of TP-2-PIE can give rise to an abrupt increase in both J_{SC} and *FF*. However, the performance of the device deteriorated if the fraction of TP-2-PIE was further increased.

A quick way to analyze the change in *FF* is to evaluate the R_S and R_{SH} variation of the devices, which can be estimated from the reciprocal of the slope for *J–V* curves.[36] It was revealed from Table 1 that the R_S of the devices decreased gradually upon the addition of TP-2-PIE component, but it was increased again if the fraction of TP-2-PIE was further increased (see Table 1**)**. The lowest R_S value was 4.79 Ω obtained in 15 wt% of TP-2-PIE component in donor. At the same time, a substantial rise in R_{SH} of the devices was found as the TP-2-PIE component was added. An optimized value of $R_{SH} = 6.97 \times 10^2$ Ω was obtained at a relatively low fraction of 10 wt% TP-2-PIE in donor. The reduction of R_S and the increase in R_{SH} contributed to the improvement in *FF*.[37] Overall, the optimized *FF* was found in 10 wt% of TP-2-PIE component in donor with over 7% improvement. The reduction in R_S indicates a better contact at the electrode of the devices if the TP-2-PIE component was added in donors. The in-depth physical mechanism in relation with the TP-2-PIE component and the device physics is subject to a thorough investigation.

2.2. Excitation Generation, Dissociation, and Energy Transfer Processes in the Devices

To understand the variation in photocurrent, external quantum efficiencies (EQEs) of the control and the device having 10 wt% of TP-2-PIE in donor were examined (see **Figure 4a)** (EQEs of the whole set of devices can be found in Figure S3, Supporting Information.) There is a distinct increase in photocurrent between 430 and 510 nm spectral ranges from the device having TP-2-PIE component. Obviously, the complementary absorption of TP-2-PIE component contributed to the enhancement of photo-harvesting in this range (Figure 3b). The integrating current (J_{int}) can be further determined to be $J_{int} = 17.13$ mA cm^{-2} for the control and 17.64 mA cm^{-2} for the device having 10 wt% of TP-2-PIE in donor, which are comparable to the J_{SC} measured from the devices (Table 1). The better photo-harvesting increased the photocurrent output from the device having 10 wt% of TP-2-PIE in donor.

Organic photovoltaic device performance is closely related to exciton formation, dissociation, and charge-separation processes. Photoluminescence (PL) can be an indication to probe a photo-excited exciton-formation process. PL spectra from varying fractions of PTB7-Th:TP-2-PIE blends were measured by exciting at $\lambda_{ex} = 475$ nm (Figure 4b). It can be clearly seen that the pristine TP-2-PIE film emits around 677 nm, while PL from pristine PTB7-Th film was quite different from that from the TP-2-PIE film, in which the latter exhibited a broad emission around ≈837 nm with a shoulder near ≈765 nm. The center emission was about 160 nm away from the PL emission of the TP-2-PIE specimen.

From Figure 4b, it was found that the intensities of the PL were progressively enhanced as the TP-2-PIE component was added gradually into the PTB7-Th matrix, and the emission profiles from the blends remained similar to that from the pristine PTB7-Th. This indicates that the TP-2-PIE component had no contribution to the PL spectra of the blends, even though the excitation wavelength (475 nm) was close to the maximum absorption for the TP-2-PIE (a minimum absorption for PTB7-Th). Only PTB7-Th emission can be observed in the PTB7-Th:TP-2-PIE–mixed specimens. However, the peak positions shift gradually to the blue as the fraction of TP-2-PIE increased. It peaks at 826 nm for the specimen with 30 wt% TP-2-PIE in donor with about a 10 nm shift (see Figure 4b).

If comparing the absorption spectrum for the PTB7-Th and the PL spectrum for the TP-2-PIE shown in Figure 4c, it was discovered that the two are heavily overlapped in the region from 600 to 770 nm. This implies that an energy transfer channel between the TP-2-PIE and PTB7-Th components could be opened, which allows transferring the excitation energy in TP-2-PIE to the adjacent PTB7-Th species to enhance PL emission from PTB7-Th. The time-resolved PL (TRPL) spectra of the blends were also evaluated and shown in Figure S4, Supporting Information, which can be fitted by a double exponential decay process with a fast (τ_1) and a slow (τ_2) lifetime as listed in Table S1, Supporting Information. The average decay times (τ_{avg}) of the blends increased progressively from 0.87 to 1.31 ns as the TP-2-PIE concentrations were increased. This also supports the energy transfer mechanism between the two donors.

The missing of TP-2-PIE emission, the enhancement of PTB7-Th emission, and the extended PL decay times when increasing TP-2-PIE concentration in the blends all form evidence for the energy transfer between the TP-2-PIE and PTB7-Th. The existence of such energy transfer would lead to extra exciton

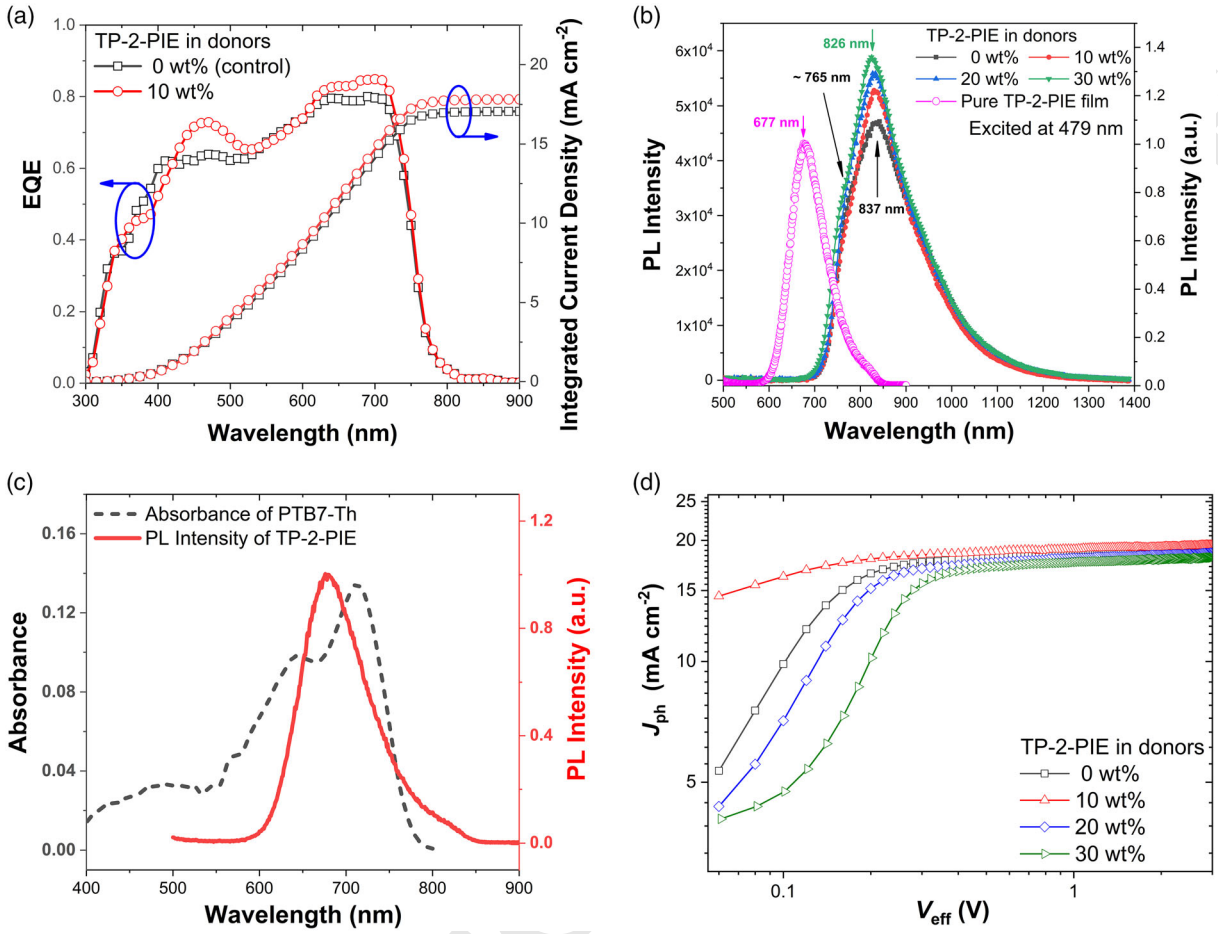

Figure 4. a) External quantum efficiency (EQE) spectra of the cells having different fractions of TP-2-PIE as indicated; b) steady-state photoluminescence (PL) spectra of PTB7-Th:TP-2-PIE films; c) comparison of PL spectrum of a TP-2-PIE film and the absorption spectrum of a PTB7-Th film; d) photocurrent density versus effective voltage characteristics of ternary devices having different fraction of TP-2-PIE additive.

formation in the donor layer, which could potentially enhance photocurrent generation in the devices.

The carrier generation and recombination processes of the active layers were analyzed through dark and illuminated J–V characteristics of the devices. In photocurrent generation process, the generation rate (G) of charge carriers can be evaluated experimentally. The photocurrent (J_{ph}) can be obtained by $J_{ph} = J_L - J_D$, where J_L and J_D are the current densities measured under a solar simulator light illumination and in the dark, respectively.[38] If plotting J_{ph} against applied voltage (V), a compensation voltage V_0 can be determined at $J_{ph} = 0$.[39] An effective voltage (V_{eff}) can therefore be obtained through $V_{eff} = V_0 - V$. A relation between J_{ph} versus V_{eff} is represented in Figure 4d.

It can be seen from Figure 4d that as V_{eff} increased, J_{ph} gradually saturated, showing that the bounded e–h pairs (the excitons) were separated into free charge carriers. A saturation current density (J_{sat}) was reached at a relatively high V_{eff} ($V_{eff} > 2$ V). In this work, J_{sat} values were taken at $V_{eff} = 3$ V and are listed in **Table 2**. It was interesting to find that the J_{sat} values are 20.10 and 19.25 mA cm^{-2} for the devices with 5 and the 10 wt % TP-2-PIE in donors, which are substantially higher than the J_{sat} value of 18.89 mA cm^{-2} from the binary device without TP-2-PIE. However, the J_{sat} dropped if the TP-2-PIE component was over 20%. This indicates that only a small fraction of the

Table 2. Maximum exciton generation rate (G_{max}) and charge dissociation probabilities P(E, T) of devices with different weight ratio of TP-2-PIE in donors.

PTB7-Th:TP-2-PIE:$PC_{71}BM$ (weight ratio)	J_{sat} at 3 V [mA cm^{-2}]	$G_{max} \times 10^{28}$ [m^{-3}s^{-1}]	$P_1(E,T)$[a)] [%]	$P_2(E,T)$[b)] [%]
1.00:0.00:1.5	18.89	1.18	90.8	69.4
0.95:0.05:1.5	20.10	1.26	91.1	71.1
0.90:0.10:1.5	19.25	1.20	93.1	75.1
0.85:0.15:1.5	19.10	1.19	91.7	70.9
0.80:0.20:1.5	17.64	1.10	87.9	69.9
0.75:0.25:1.5	17.35	1.08	87.1	69.7
0.70:0.30:1.5	17.13	1.07	84.4	68.5

[a)]The dissociation probability at short-circuit condition; [b)]the dissociation probability at maximum power condition.

TP-2-PIE component present in the active layer could significantly enhance J_{sat}.

Supposing no recombination of free charge carriers if space–charge effects can be neglected, the J_{sat} could be transported and collected by the electrodes. The J_{sat} through the external circuit can be given by $J_{ph} = qLG$, where q is the elementary electric charge and L is the thickness of the active layer.[39,40] The maximum exciton generation rate (G_{max}) can be evaluated using $J_{sat} = qLG_{max}$ and the results are also listed in Table 2. It was found that in ternary devices with a relatively low fraction (5–15 wt%) of TP-2-PIE in donors, the G_{max} is higher than that for the control device. This indicates that the charge separations were enhanced.

Assuming that charge is fully separated at J_{sat}, a dissociation probability $P(E,T) = J_{ph}/J_{sat}$ can be defined, where $P_1(E,T)$ and $P_2(E,T)$ are the dissociation probabilities at a short-circuit condition and at a maximum power condition, respectively.[39] The calculated values are listed in Table 2. The highest values for $P_1 = 93.1\%$ and $P_2 = 75.1\%$ are from the ternary device having 10 wt% TP-2-PIE in donors, indicating the most efficient condition for charge separation and dissociation. This is in good agreement with what has been found that the device having 10 wt% of TP-2-PIE performed the best in photovoltaic response as seen in Table 1.

The results indicate that only a small fraction of TP-2-PIE having an extended absorption along with its energy transfer is enough to enhance charge dissociation, which explains well the enhancement of photocurrent in photovoltaic devices.

2.3. The Device Physics in Relation to the Molecular Interaction, Morphology, and Charge Carrier Transport of the Active Layers

The charge generation and separation in a donor-/acceptor-blended organic polymer matrix are generally complicated, which can be closely related to the morphology of the blended system, in particular, the formation of two-component-blended domains. The molecular interactions can be a key factor, which may alter the miscibility of the components and hence the phase separation.

In the current investigation, surface morphologies of the blended active layers with different concentration of the TP-2-PIE component were explored using atomic force microscopy (AFM) as shown in **Figure 5**. It was interesting to observe from the topographic images that the introduction of TP-2-PIE component into the initial binary (PTB7-Th:$PC_{71}BM$) film is able to change the surface morphology distinctly. The surface of the control film was relatively smooth, but granule-like structures were developed as the TP-2-PIE fraction was increased. To quantify such a change, root-mean-square roughness (R_{RMS}) of the active layers was evaluated, which appeared to increase gradually from 3.2 nm for the control specimen up to 15.0 nm for the layer having 30 wt% TP-2-PIE in donors. That is, the surface became rougher with structure developed as the TP-2-PIE fraction was increased. Obviously, the changes in surface morphology were induced by the introduction of LC TP-2-PIE component. The changes in surface morphology might reflect a change of morphology in the bulk, such as molecular aggregation or phase separation. It is therefore useful to analyze the molecular interaction to see how these blended domains formed.

Due to the PTB7-Th polymer being almost amorphous in nature, no distinct crystalline diffractions can be observed in wide-angle X-Ray diffraction. A direct observation of changes in structural order is difficult. Nevertheless, with the help of a Flory–Huggins model,[41–43] it is possible to evaluate the molecular interaction and hence the miscibility in multicomponents. Therefore, the phase separation of a blended system can be analyzed.

According to Flory–Huggins theory, an interaction parameter (χ), relating a thermodynamic driving force to the morphology formations in an amorphous polymeric system, is a particularly important value in the control of miscibility, phase separation, and morphological stability.[44,45] This could help us to investigate the role of the TP-2-PIE molecule on the microstructural morphology and the phase separation of the donor/acceptor blends.[46]

The Flory–Huggins interaction parameter χ can be related to the cohesive energy density of the components for an amorphous polymer—small molecule blend system through Equation (1).[47,48]

$$\chi_{ij} = \frac{V_0}{RT}(\delta_i - \delta_j)^2 + 0.34 \quad (1)$$

where χ_{ij} is the interaction parameter for the component i and j, respectively, V_0 is the geometric mean of the polymer segment molar volume, R is the gas constant, T is the absolute temperature in K, and the δ_i and δ_j are the Hildebrand solubility parameters for the components i and j, respectively. The squared difference $(\delta_i - \delta_j)^2$ between components is a measure of the increase in energy on mixing. And, 0.34 represents a correction factor for entropic contributions in a polymer solution system.

In this work, the solubility parameters were estimated through surface energy measurement as δ value is the square root of the surface energy (γ_s) ($\delta = K\gamma_s^{1/2}$) and K is a universal proportionality constant, which can be determined by measuring a known material.[49] The surface energy γ_s can be obtained experimentally by measuring the contact angles as described in Supporting Information. The contact angles for films of the pristine or blended donor(s), as well as the acceptor, are shown in **Figure 6** (and Table S2, Supporting Information). The γ_s values were calculated and tabulated in **Table 3**. Therefore, the parameter χ values were analyzed based on the mixed donor (PTB7-Th with TP-2-PIE) and the accepter ($PC_{71}BM$) components, and the resulted can be found in Table 3.

It can be seen clearly that the addition of TP-2-PIE into the PTB7-Th matrix led to a gradual increase in the surface contact angles to the testing liquid. Hence, the γ_s value decreased gradually from 29.05 mN m^{-1} for the pristine PTB7-Th layer down to about 24.24 mN m^{-1} for the donor layer having 30 wt% of TP-2-PIE component. This reduced the δ values accordingly. The γ_s value for the donor layer having 30 wt% of TP-2-PIE component is much lower than that for the $PC_{71}BM$ (41.58 mN m^{-1}). As a result, the differences in solubility parameters ($\Delta\delta$) between the donor and acceptor increased, that is, from $\Delta\delta = 3.34$ to 5.05, as the fraction of TP-2-PIE component increased. Consequently, an increase of TP-2-PIE concentration substantially enhanced the

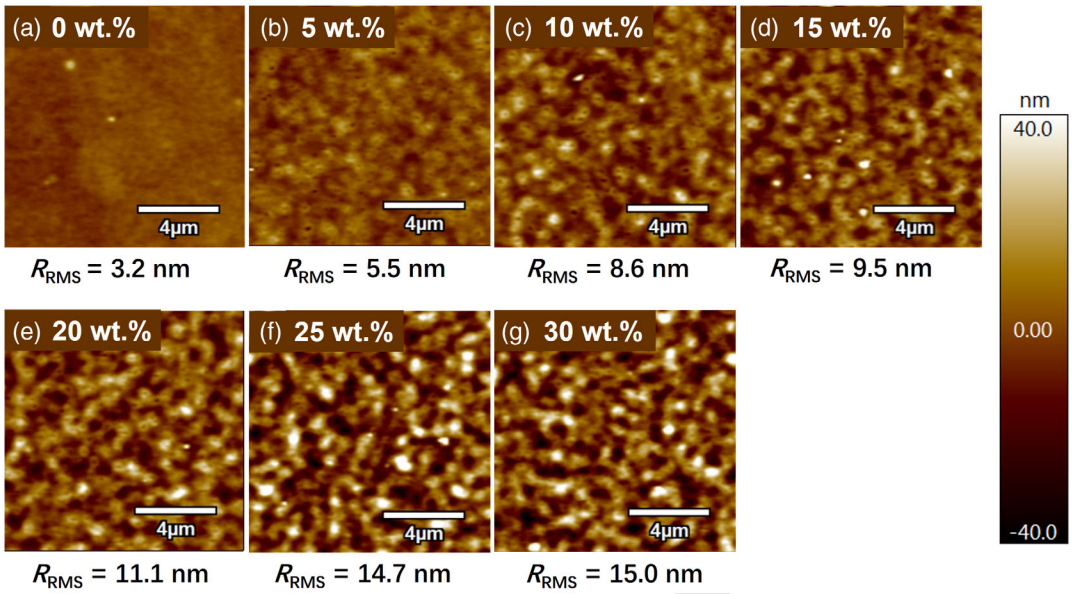

Q9 **Figure 5.** Tapping-mode atomic force microscopy (AFM) topography height images of a) PTB7-Th:$PC_{71}BM$ as-cast, b–g) PTB7-Th:$PC_{71}BM$ with different weight fractions of TP-2-PIE in donors as indicated. Root-mean-square roughness (R_{RMS}) is marked below each graph.

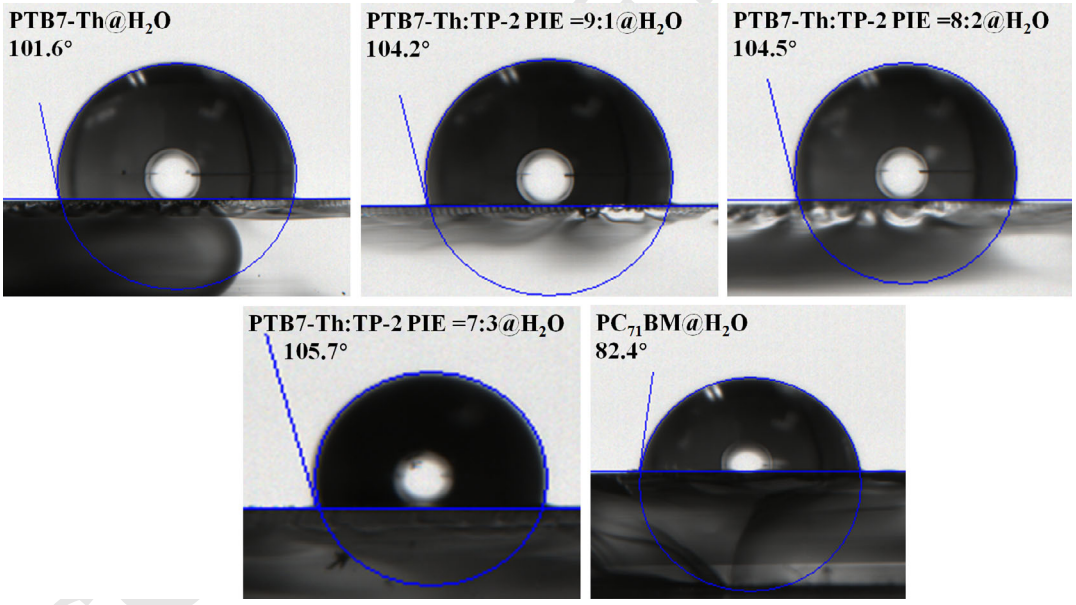

Q11 **Figure 6.** Contact angles of different ratios of TP-2-PIE in donors and PCBM on H_2O.

Table 3. The summarized surface free energy γ_s, solubility parameters δ, and Flory–Huggins interaction parameters χ of different ratios of TP-2-PIE in donors and PCBM.

i (weight ratio)	γ_s [mN m^{-1}]	δ [$MPa^{1/2}$]	$\chi_{(i,\ PC71BM)}$
PTB7-Th:TP-2-PIE = 10:0	29.05	19.77	0.68
PTB7-Th:TP-2-PIE = 9:1	25.90	18.67	1.22
PTB7-Th:TP-2-PIE = 8:2	25.63	18.57	1.27
PTB7-Th:TP-2-PIE = 7:3	24.24	18.06	1.57
$PC_{71}BM$	41.58	23.11	n/a

interaction parameter $\chi_{donor/acceptor}$. The $\chi_{PTB7\text{-}Th/PCBM}$ took a value of 0.68 for the binary PTB7-Th:$PC_{71}BM$ pair; while the $\chi_{(PTB7\text{-}Th:TP\text{-}2\text{-}PIE\,=\,7:3)/PCBM}$ raised to 1.57 for the ternary mixed donor (PTB7-Th:TP-2-PIE = 7:3) and $PC_{71}BM$ pair.

Flory–Huggins interaction parameters χ plays an important role in the morphology formation.[48,50,51] An increase in χ value would lead to a decrease in miscibility of the components, which determines the driving force for phase separation. In comparison of the χ values with the AFM images in Figure 5, it is found that a lower χ value as in the control layer has a relatively good miscibility between the D–A components demonstrating a smooth

surface with less phase separation. A structured surface with higher roughness corresponds to a larger χ value for a reduced miscibility in the active layer having a TP-2-PIE component, which displayed an enhancement in phase separation, or the phase-separated domain growing larger. The χ value analyses agree well with the experimental observations.

Since a good miscibility with a low χ value could lead to a low domain purity,[52] a higher χ value is therefore beneficial for a higher degree of phase separation forming domains with a relatively high purity. Phase separation with high domain purity has been found to offer charge-transporting channels more efficiently, which is beneficial for the photovoltaic performance.[51] However, our ternary devices performed well only when the TP-2-PIE component was less than 20% (see Table 1). Although a further increase in TP-2-PIE concentration to over 25 wt% enhanced the phase separation, the device performance deteriorated. For example, the active layer having 30 wt% of TP-2-PIE component was highly phase separated (Figure 5g), and the device efficiency was substantially reduced (Table 1). Further charge-transporting processes were investigated to understand this.

Q12 Single-carrier hole-only (ITO/PEDOT:PSS/Active layer/Au) and electron-only (ITO/ZnO/Active layer/Al) devices having different fractions of TP-2-PIE component in the active layer were fabricated. *J*–*V* characteristics of these ternary devices were plotted on a double logarithmic scale as shown in **Figure 7**a,b. The hole or electron mobility in actively layers can be estimated based on the space-charge limited current (SCLC) method similar to our previous work.[15,53]

It can be seen from Figure 7a,b that J increased linearly against V (i.e., $J \propto V$) in all devices at low voltage bias regions, indicating that an ohmic contact was fulfilled. As the bias voltage increased in hole-only devices (see Figure 7a, the current went into a trap-filled limited region first, followed by the third region having a quadratic voltage dependence ($J \propto V^n$, $n = 2$), that is, an SCLC was reached. However, in the electron-only devices, no trap-filled limited current can be observed in Figure 7b. As the bias voltage increased, current went directly into a trap-free SCLC region with a quadratic voltage dependence ($J \propto V^2$). In the SCLC region, the charge carrier mobility can be obtained through the Mott–Gurney equation as seen in Equation (2), which is combined with the Poole–Frenkel expression [$\mu = \mu_0 \exp(\gamma\sqrt{F})$] to take account of the field dependency and the imperfect quadratic relation.[15,38]

$$J_{\mathrm{SCLC}} = \frac{9}{8}\frac{\varepsilon_0\varepsilon_r\mu_0}{L}\exp(0.891\gamma\sqrt{F})F^2 \quad (2)$$

In Equation (2), F is the applied electric field defined as $F = V/L$ and L is the thickness of the active layer, which is 100 nm in this work; ε and ε_0 are the relative and vacuum permittivity of the materials, respectively, and we take $\varepsilon_r = 3$ for organic materials in this work; μ_0 is the carrier mobility at zero electric field; and γ is a constant. The γ and μ_0 can be obtained from the slope and the intercept of $\ln(J/F^2)$ versus $F^{1/2}$ plot in the high-field region (see Figure S5, Supporting Information) so that the values of hole mobility (μ_h) and electron mobility (μ_e) can be calculated at an electric field of 10^6 Vm^{-1}.[15] The balance of the hole and electron transport can be evaluated via a ratio of μ_e/μ_h calculated for the corresponding devices. These results are listed in **Table 4**. As the trap-filled limited current occurred solely in the hole-only devices, the densities of trap states (n_t) were calculated only for holes following a relation of $V_{\mathrm{TFL}} = qn_tL^2/2\varepsilon\varepsilon_0$, where V_{TFL} is the trap-filled limited voltage and q is the elementary charge. These results are also listed in **Table 4**.

It is interesting to see from the Table 4 that the TP-2-PIE component had a relatively weak effect on the μ_e of the device. The μ_e showed a slight increase in the device having 10 wt% of TP-2-PIE in donor with a μ_e value of 3.8×10^{-4}. However, the TP-2-PIE component was able to tune μ_h substantially. The μ_h increased gradually as the TP-2-PIE concentrations were increased. The μ_h values enhanced monotonically from 6.8×10^{-4} cm^{2}V^{-1}s^{-1} for the control device to 1.1×10^{-3} cm^{2}V^{-1}s^{-1} for the device having 30 wt% of TP-2-PIE in donor.

The increase in charge carrier mobilities is in good agreement with the change in Flory–Huggins interaction parameters χ of the D–A pairs (see Table 3). It is very interesting that the gradual increase in μ_h was coincident with the increase in χ values with a decreased miscibility and an enhanced phase separation and/or domain purity.

It is known that the DLC TP-2-PIE is able to crystallize at room temperature and forms LC phase at elevated temperatures. More importantly, such a DLC molecule possesses a self-organization property, which can be orientated face-on based on molecular π–π stacking.[20,31,33] This may induce a higher degree of structural order in organic polymer systems.[41,54]

Based on the earlier analyses, the changing in morphology may be explained as follows. To simplify the complicated ternary system, we start from two mixed phases for the control (binary) specimen: one phase was dominated by PTB7-Th polymer (donor) and the other phase was dominated by $PC_{71}BM$ (acceptor). Both phases are mixed with D/A components, but with different purities. This can be illustrated in **Figure 8**.

From the molecular structures, it was expected that the TP-2-PIE component would mix better with polymer PTB7-Th than with fullerene $PC_{71}BM$. Due to the Flory–Huggins interaction parameter that became larger when the fraction of TP-2-PIE component was increased, the D–A phase separation was promoted. A highly order TP-2-PIE component would induce more ordered structure in the donor-dominated domain. It not only developed ordered structures and resulted in phase separation, but might also enhance the purity in donor-dominated PTB7-Th:TP-2-PIE phase as shown in Figure 8. A phase-separated morphology consisting of higher degree of order in structure with a good domain purity is expected to offer a good charge transport channel and improve the charge carrier mobility.[51] Coincidently, in our experiments, the μ_h of the active layer was gradually increased as the TP-2-PIE concentration increased. However, the μ_e of the active layer was less affected, which increased slightly as the TP-2-PIE concentration increased but then reduced again if the fraction of TP-2-PIE component was further increased. This indicates that the TP-2-PIE component main functioned in the donor-dominated phase.

In this work, although the μ_h of the device was substantially increased due to the addition of TP-2-PIE component, the photovoltaic performance was first improved and then deteriorated as the fraction of TP-2-PIE component increased. This can be understood by the balance between the hole and electron

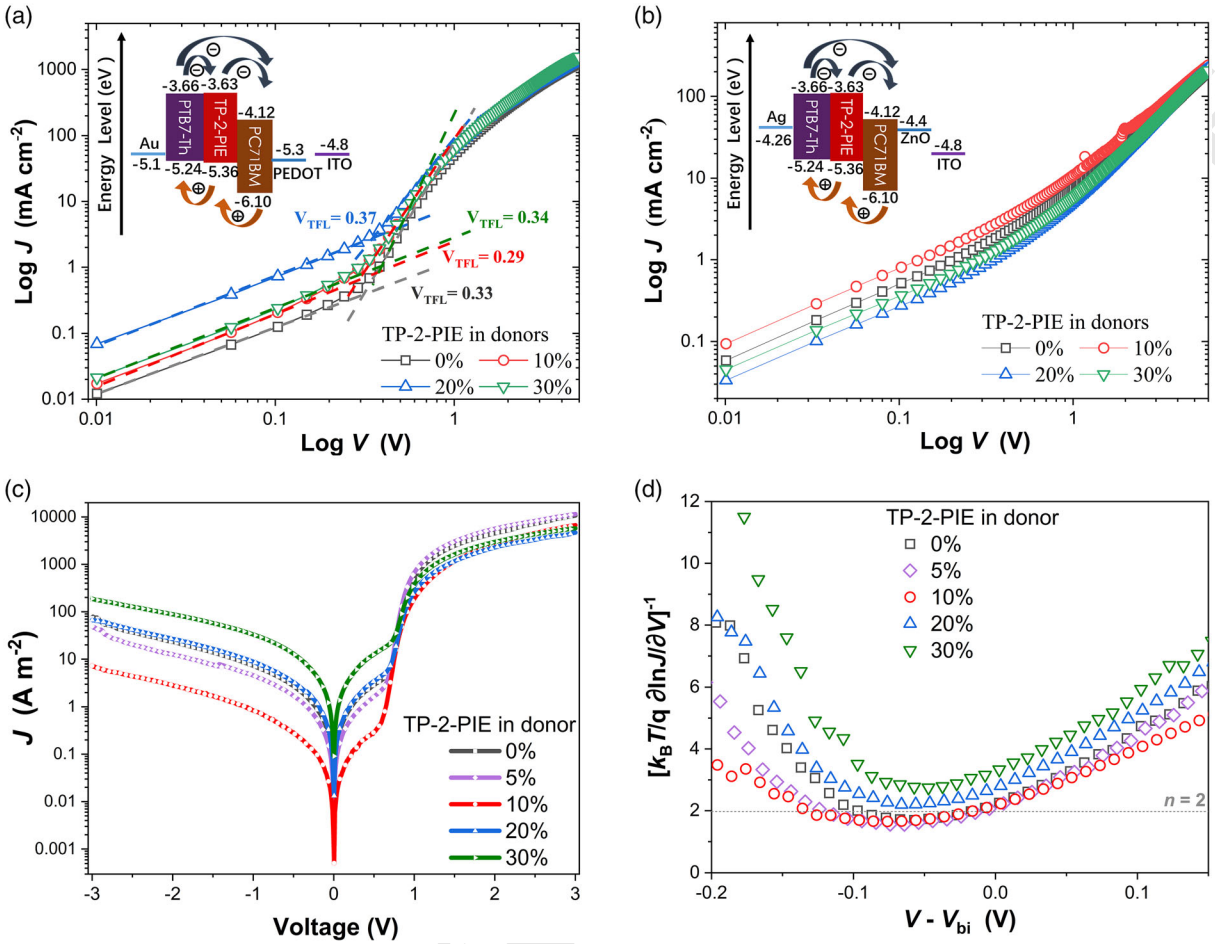

Figure 7. *J–V* characteristics of a) hole-only and b) electron-only devices plotted on a double logarithmic scale; c) dark *J–V* and d) *n–V* characteristics are obtained from the photovoltaic devices. (The TP-2-PIE fractions indicated are weight fractions).

Table 4. Hole (μ_h) and electron (μ_e) mobilities measured by space-charge limited current (SCLC) method from devices having different fraction of TP-2-PIE in donors.

PTB7-Th: TP-2-PIE: $PC_{71}BM$ (weight ratio)	μ_h [$cm^2V^{-1}s^{-1}$]	μ_e [$cm^2V^{-1}s^{-1}$]	μ_h/μ_e	n_t[a)] [cm^{-3}]
1.0:0:1.5	6.8×10^{-4}	2.0×10^{-4}	3.4	1.1×10^{16}
0.9:0.1:1.5	7.6×10^{-4}	3.8×10^{-4}	2.0	9.6×10^{15}
0.8:0.2:1.5	9.6×10^{-4}	1.9×10^{-4}	5.1	1.2×10^{16}
0.7:0.3:1.5	1.1×10^{-3}	1.5×10^{-4}	7.3	1.1×10^{16}

[a)] Density of trap states was calculated from the hole-only devices.

mobilities. It can be seen from Table 4 that the device with 10 wt% TP-2-PIE in donor demonstrated the lowest μ_h/μ_e ratio of 2.0. It means that a symmetrical electric field distribution could be established in the active layer to reach a transport balance. It is the balance in charge carrier mobility, which contributes to the increase in J_{sc} and *FF* of the device.[55,56] The unbalanced carrier mobilities would result in a space charge accumulation, which would reduce the J_{sc} and enhanced the recombination at the interface leading to low *FF*.[56]

Further semiconducting physical analysis was carried out through the dark $J - V$ characteristics of the ternary devices, which is plotted in a semilogarithmic scale as depicted in Figure 7c. It can be seen from Figure 7c that the current density fell into three distinct regions. At low voltage bias, a leakage current can be seen, which was substantially reduced when a small fraction of TP-2-PIE component was added into the active layer. However, further addition of TP-2-PIE component increased the leakage current again. The minimum leakage current was achieved in device having 10 wt% of TP-2-PIE in donor. As the bias voltage increased, but was still below the built-in voltage (V_{bi}), the *J–V* curve went into the second region, where the current is diffusion dominated and has an exponential dependence on voltage, which can be described using a classical Shockley diode equation (Equation (3)) given as follows.[57]

$$J = J_0\left[\exp\left(\frac{qV}{nk_BT}\right) - 1\right] \quad (3)$$

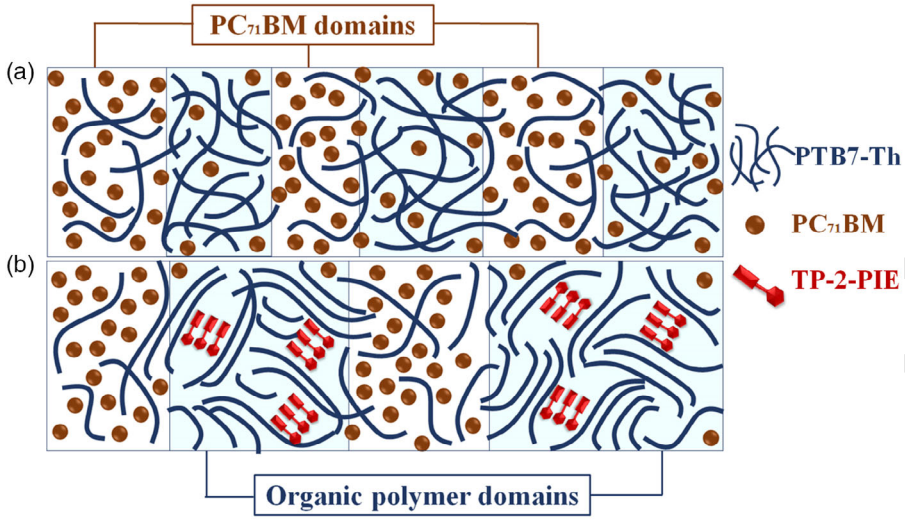

Figure 8. A schematic diagram of donor–acceptor phase separation induced by TP-2-PIE component, which induced enhanced order in organic polymer-dominated phase with enlarged area.

where J_0 is the saturation current density, n is an empirical ideality factor, k_B is the Boltzmann constant, and T is the temperature. In this work, n values were obtained by fitting experimental results using Equation (4). The results were plotted against voltage as shown in Figure 7d.

$$n = \left(\frac{k_B T}{q}\frac{\partial \ln J}{\partial V}\right)^{-1} \quad (4)$$

For organic semiconductors, n value contains important information, such as recombination and carrier transport processes. For a classical semiconducting device of an ideal p–n junction diode without traps and carrier recombination, the n is expected to be equal to unity. However, if a trap-assisted recombination process is presented, the n may deviate from 1 and take a value of 2.[57] It has been reported that the situation in a BHJ organic solar cell can be more complicated, such as for polymer:fullerene organic solar cells, and ideality factors were typically 1.3–2.0 as reported.[58–60] The deviation of the ideality factors from unity was observed in devices with traps free for both hole (donor) and electron (acceptor). Therefore, the nonideality of the dark current in BHJ organic solar cells cannot be used as an evidence for the presence of trap-assisted recombination. It can be the transport-dominating constituent in the donor:acceptor blend.[61]

It was found in this work that the addition of a small fraction of TP-2-PIE component into active is able to reduce the n value slightly from $n = 1.71$ for the control device down to $n = 1.56$ and 1.65 for the devices having 5 and 10 wt% of TP-2-PIE component in donor. However, with further increasing in TP-2-PIE concentration, the n value would increase to levels over 2. These results are in good agreement with the calculated density of trap states (n_t) as seen in Table 4. It can be clearly seen that the improvement in ideality factor of devices was correlated to the decrease in the calculated density of trap states. The confirmed recombination in these ternary devices is a trap-assisted process.

From this investigation, it was found that the TP-2-PIE component has multiple functionalities in the ternary active layer. Tuning the TP-2-PIE concentration could alter the molecular interaction and hence the phase separation and/or domain purity, which further changed the charge transport mobility and the density of trap states. A good phase separation with higher degree of structural order and a reduced density of trap states could enhance charge carrier mobility with a higher extent for hole mobility. Therefore, a mobility balance can be achieved at an optimized condition having 10 wt% of TP-2-PIE component. At the optimized condition, the ideality factor of the device was also reduced.

The molecular interaction, good phase separation or domain purity, the balance transport, and the reduced density of trap states ultimately enhance the photovoltaic performance of the ternary devices.

3. Conclusion

In this work, a D–A discotic liquid crystal organic TP-2-PIE was elaborately selected as a third component to fabricate the ternary PSCs by blending with PTB7-Th:$PC_{71}BM$ active layers. The TP-2-PIE molecule has both electron donating and accepting moieties to interact with other components as well as the ability to self-organize into a highly ordered or orientated molecular assembly to tune the morphology.

It was found that the TP-2-PIE component had no effect on V_{OC} on devices using the PTB7-Th:$PC_{71}BM$ pair, but substantially changed the J_{SC} and FF of the devices. This investigation discovered that the TP-2-PIE component has multiple functionalities in the ternary device: 1) the complementary absorption by TP-2-PIE and energy transfer between the TP-2-PIE and PTB7-Th granted the mixed donors with an extended photo-harvesting and extra exciton formation. The photocurrent and hence the J_{SC} of the devices can be enhanced; and 2) The TP-2-PIE component altered the molecular interaction quantified by the Flory–

Huggins interaction parameter leading to a better phase separation with higher domain purity in the active layers. This resulted in an enhancement of charge carrier transport with a good balance and minimized density of trap states. The ideality factor n of the devices was also lowered. These improved the overall performance of the photovoltaic devices and markedly enhanced the J_{SC} and FF of the devices.

The optimal device with 10 wt% TP-2-PIE in donors achieved a 12.6% improvement in PCE as compared with the control (binary) device. This investigation offers a better understanding with regards to the functionalities of the third component in ternary BHJ organic solar cells, which may act as a guide for further device development.

4. Experimental Section

Materials: A liquid crystal compound TP-2-PIE was synthesized and reported elsewhere.[31] PTB7-Th and $PC_{71}BM$ were purchased from 1-Material Inc. These materials were used in active layers with chemical structures which are shown in Figure 2. The 1,8-diiodooctance was obtained from TCI Inc. Silver metallic particles (99.99%) and MoO_3 (99.95%) were from ZhongNuo Advanced Material (Beijing) Technology Co. and Sigma-Aldrich, respectively. Patterned indium tin oxide (ITO)-coated glasses were purchased from South China Science & Technology Company Limited, which has a sheet resistance of 15 Ω square^{-1}. Organic solvents (AR) and other reagents were purchased from Acros if not specified.

ZnO precursor was prepared by dissolving zinc acetate dihydrate (purchased from Aladdin Inc.) into 2-methoxyethanol solvent, which was purchased from TCI Inc. Precursor for active layer (active solution) was made by co-dissolving pristine PTB7-Th or blended with TP-2-PIE as donors (10 mg mL^{-1}) and $PC_{71}BM$ as an accepter (15 mg mL^{-1}) into dichlorobenzene at a weight ratio of 1:1.5. The 1,8-diiodooctance (3 vol%) was also added to the active solution as a solvent additive.

Device Fabrication: Device fabrication procedures were as follows: ITO substrates were ultrasonically cleaned first with detergent for 24 h, which were then washed with deionized water and acetone for 20 min as each. After drying with N_2 flow, the cleaned ITO substrates were treated in O_2 plasma environment for 20 min before use. First of all, a thin layer of ZnO, the electron transporting layer, was prepared on top of the ITO substrates by spin-coating the ZnO precursor at a spinning rate of 3000 rpm for 40 s. It was followed by thermal annealing at 200 °C in air for 40 min.[62] This was then transferred into a nitrogen-filled glove box to prepare the active layer. Active layer was prepared by spin-coating the active solution at 1200 rpm for 60 s on the top of ZnO layer to form a layer having an area of 0.038 cm^2. Hole transporting layer of molybdenum trioxide (MoO_3) was deposited using a vacuum evaporator and finally a silver electrode was deposited similarly at a pressure of 1×10^{-4} Pa.

Materials and Device Measurements: Thickness of the active layers was measured using a surface profile (Ambios XP-2), which was about 100 nm. UV-vis-near-infrared (NIR) spectrophotometers (Shimadzu UV-310PS and UV2600) had been used to measure the absorption spectra of the film specimen. X-Ray diffraction patterns were taken by a Bruker D8 advance diffractometer. Steady-state and TRPL spectra were measured using a PL spectrometer (Edinburgh Instruments FLS 1000) using a NIR photomultiplier tube (Hamamatsu R5509-73 PMT) as detector with liquid nitrogen cooling for 2 h before measurement. The emissions were corrected for the instrumental spectral response. The transient emission was excited with a 406 nm laser diode. The contact angles were measured optically through a static sessile–drop method using an automatic goniometer and surface energies were calculated using a droplet analyzer (Guangdong Hokuto Instrument Co. & Ltd., CA200).

Current–voltage characteristics of the devices were measured using a source measure unit (Agilent B2902A). Photovoltaic responses were obtained under a standard illumination of AM 1.5G solar irradiation at 100 mW cm^{-2} from a solar simulator (Abet Sun 2000). EQEs of the solar cells were evaluated through a solar cell quantum efficiency measurement system (Zolix Solar Cell Scan 100).

Supporting Information

Supporting Information is available from the Wiley Online Library or from the author.

Acknowledgements

This work is supported by National Natural Science Foundation of China (Grant nos. 11474017, 61874008, and 62174011). The authors would like to thank the medium instrumental lab in chemistry, Peking University for their kind assistance in partial PL measurements.

Conflict of Interest

The authors declare no conflict of interest.

Data Availability Statement

The data that support the findings of this study are available from the corresponding author upon reasonable request.

Keywords

charge carrier mobility, discotic, energy transfer, Flory–Huggins interaction parameter, phase separation, photovoltaics, polymer solar cells

Received: January 31, 2022
Revised: February 28, 2022
Published online:

[1] Z. A. Li, C.-C. Chueh, A. K. Y. Jen, *Prog. Polym. Sci.* **2019**, *99*, 101175.
[2] Y. Li, *Acc. Chem. Res.* **2012**, *45*, 723.
[3] S. Lee, D. Jeong, C. Kim, C. Lee, H. Kang, H. Y. Woo, B. J. Kim, *ACS Nano* **2020**, *14*, 14493.
[4] R. S. Gurney, D. G. Lidzey, T. Wang, *Rep. Prog. Phys.* **2019**, *82*, 036601.
[5] X. Wan, C. Li, M. Zhang, Y. Chen, *Chem. Soc. Rev.* **2020**, *49*, 2828.
[6] F. Zhao, H. Zhang, R. Zhang, J. Yuan, D. He, Y. Zou, F. Gao, *Adv. Mater.* **2020**, *10*, 2002746.
[7] L. Ma, S. Zhang, J. Wang, Y. Xu, J. Hou, *Chem. Commun.* **2020**, *56*, 14337.
[8] Y. Wang, J. Lee, X. Hou, C. Labanti, J. Yan, E. Mazzolini, A. Parhar, J. Nelson, J. S. Kim, Z. Li, *Adv. Mater.* **2020**, *11*, 2003002.
[9] P. Cheng, X. Zhan, *Mater. Horiz.* **2015**, *2*, 462.
[10] L. Lu, M. A. Kelly, W. You, L. Yu, *Nat. Photonics* **2015**, *9*, 491.
[11] T. Ameri, P. Khoram, J. Min, C. J. Brabec, *Adv. Mater.* **2013**, *25*, 4245.
[12] L. Yang, L. Yan, W. You, *J. Phys. Chem. Lett.* **2013**, *4*, 1802.
[13] D. Adam, P. Schuhmacher, J. Simmerer, L. Häussling, K. Siemensmeyer, K. H. Etzbachi, H. Ringsdorf, D. Haarer, *Nature* **1994**, *371*, 141.
[14] A. M. V. D. Craats, J. M. Warman, A. Fechtenkötter, J. D. Brand, M. A. Harbison, K. Müllen, *Adv. Mater.* **1999**, *11*, 1469.
[15] H. Zhao, Z. He, M. Xu, C. Liang, S. Kumar, *Phys. Chem. Chem. Phys.* **2016**, *18*, 8554.

[16] T. Wohrle, I. Wurzbach, J. Kirres, A. Kostidou, N. Kapernaum, J. Litterscheidt, J. C. Haenle, P. Staffeld, A. Baro, F. Giesselmann, S. Laschat, *Chem. Rev.* **2016**, *116*, 1139.
[17] C. W. Tang, *Appl. Phys. Lett.* **1986**, *48*, 183.
[18] L. Schmidt-Mende, A. Fechtenkotter, K. Mullen, E. Moons, R. H. Friend, J. D. MacKenzie, *Science* **2001**, *293*, 1119.
[19] S. Jeong, Y. Kwon, B.-D. Choi, H. Ade, Y. S. Han, *Appl. Phys. Lett.* **2010**, *96*, 183305.
[20] J. Zhang, Y. Zhang, J. Fang, K. Lu, Z. Wang, W. Ma, Z. Wei, *J. Am. Chem. Soc.* **2015**, *137*, 8176.
[21] K. Sun, Z. Xiao, S. Lu, W. Zajaczkowski, W. Pisula, E. Hanssen, J. M. White, R. M. Williamson, J. Subbiah, J. Ouyang, A. B. Holmes, W. W. Wong, D. J. Jones, *Nat. Commun.* **2015**, *6*, 6013.
[22] X. Ma, F. Zhang, Q. An, Q. Sun, M. Zhang, J. Miao, Z. Hu, J. Zhang, *J. Mater. Chem. A* **2017**, *5*, 13145.
[23] C. Yan, H. Tang, R. Ma, M. Zhang, T. Liu, J. Lv, J. Huang, Y. Yang, T. Xu, Z. Kan, H. Yan, F. Liu, S. Lu, G. Li, *Adv. Sci.* **2020**, *7*, 2000149.
[24] K. Chong, X. Xu, H. Meng, J. Xue, L. Yu, W. Ma, Q. Peng, *Adv. Mater.* **2022**, https://doi.org/10.1002/adma.202109516e2109516.
[25] M. T. Dang, L. Hirsch, G. Wantz, J. D. Wuest, *Chem. Rev.* **2013**, *113*, 3734.
[26] K. Yuan, L. Chen, Y. Chen, *J. Mater. Chem. C* **2014**, *2*, 3835.
[27] M. A. Ruderer, P. Müller-Buschbaum, *Soft Matter* **2011**, *7*, 5482.
[28] M. A. Ruderer, S. Guo, R. Meier, H.-Y. Chiang, V. Körstgens, J. Wiedersich, J. Perlich, S. V. Roth, P. Müller-Buschbaum, *Adv. Funct. Mater.* **2011**, *21*, 3382.
[29] G. Li, Y. Yao, H. Yang, V. Shrotriya, G. Yang, Y. Yang, *Adv. Funct. Mater.* **2007**, *17*, 1636.
[30] A. K. K. Kyaw, D. H. Wang, C. Luo, Y. Cao, T.-Q. Nguyen, G. C. Bazan, A. J. Heeger, *Adv. Mater.* **2014**, *4*, 1301469.
[31] X. Kong, H. Gong, P. Liu, W. Yao, Z. Liu, G. Wang, S. Zhang, Z. He, *New J. Chem.* **2018**, *42*, 3211.
[32] P. E. Hartnett, S. M. Dyar, E. A. Margulies, L. E. Shoer, A. W. Cook, S. W. Eaton, T. J. Marks, M. R. Wasielewski, *Chem. Sci.* **2015**, *6*, 402.
[33] J. Wang, Z. He, Y. Zhang, H. Zhao, C. Zhang, X. Kong, L. Mu, C. Liang, *Thin Solid Films* **2010**, *518*, 1973.
[34] J. Li, Z. He, H. Zhao, H. Gopee, X. Kong, M. Xu, X. An, X. Jing, A. N. Cammidge, *Pure Appl. Chem.* **2010**, *82*, 1993.
[35] N. K. Elumalai, A. Uddin, *Energy Environ. Sci.* **2016**, *9*, 391.
[36] A. Moliton, J.-M. Nunzi, *Polym. Int.* **2006**, *55*, 583.
[37] J. D. Servaites, S. Yeganeh, T. J. Marks, M. A. Ratner, *Adv. Funct. Mater.* **2010**, *20*, 97.
[38] Z. Guo, Z. He, M. Sun, H. Zhang, Y. Xu, X. Li, C. Liang, X. Jing, *Polymer* **2018**, *153*, 398.
[39] V. D. Mihailetchi, L. J. Koster, J. C. Hummelen, P. W. Blom, *Phys. Rev. Lett.* **2004**, *93*, 216601.
[40] V. D. Mihailetchi, J. Wildeman, P. W. Blom, *Phys. Rev. Lett.* **2005**, *94*, 126602.
[41] P. J. Flory, *Principles of Polymer Chemistry*, Cornell University Press, Ithaca, NY **1953**.
[42] P. J. Flory, *J. Chem. Phys.* **1942**, *10*, 51.
[43] M. L. Huggins, *J. Chem. Phys.* **1941**, *9*, 440.
[44] *Polymer Handbook*, 4th ed. (Eds: J. Brandrup, Immergut, E. H., Grulke, E. A.), Wiley, John Wiley & Sons, New York **1999**.
[45] M. Gao, Z. Liang, Y. Geng, L. Ye, *Chem. Commun.* **2020**, *56*, 12463.
[46] L. Zhang, X. Xu, B. Lin, H. Zhao, T. Li, J. Xin, Z. Bi, G. Qiu, S. Guo, K. Zhou, X. Zhan, W. Ma, *Adv. Mater.* **2018**, *30*, e1805041.
[47] J. A. Emerson, D. T. W. Toolan, J. R. Howse, E. M. Furst, T. H. Epps, *Macromolecules* **2013**, *46*, 6533.
[48] S. Nilsson, A. Bernasik, A. Budkowski, E. Moons, *Macromolecules* **2007**, *40*, 8291.
[49] S. Kouijzer, J. J. Michels, M. van den Berg, V. S. Gevaerts, M. Turbiez, M. M. Wienk, R. A. Janssen, *J. Am. Chem. Soc.* **2013**, *135*, 12057.
[50] R. Wang, J. Yuan, R. Wang, G. Han, T. Huang, W. Huang, J. Xue, H. C. Wang, C. Zhang, C. Zhu, P. Cheng, D. Meng, Y. Yi, K. H. Wei, Y. Zou, Y. Yang, *Adv. Mater.* **2019**, *31*, e1904215.
[51] L. Ye, H. Hu, M. Ghasemi, T. Wang, B. A. Collins, J. H. Kim, K. Jiang, J. H. Carpenter, H. Li, Z. Li, T. McAfee, J. Zhao, X. Chen, J. L. Y. Lai, T. Ma, J. L. Bredas, H. Yan, H. Ade, *Nat. Mater.* **2018**, *17*, 253.
[52] B. P. Lyons, N. Clarke, C. Groves, *Energy Environ. Sci.* **2012**, *5*, 7657.
[53] X. Zhang, Z. He, C. Liang, Y. Wang, Q. Zhuang, Z. Han, *Appl. Phys. Lett.* **2013**, *103*, 043306.
[54] G. Li, V. Shrotriya, J. Huang, Y. Yao, T. Moriarty, K. Emery, Y. Yang, *Nat. Mater.* **2005**, *4*, 864.
[55] W. Tress, A. Petrich, M. Hummert, M. Hein, K. Leo, M. Riede, *Appl. Phys. Lett.* **2011**, *98*, 063301.
[56] L. J. A. Koster, V. D. Mihailetchi, P. W. M. Blom, *Appl. Phys. Lett.* **2006**, *88*, 052104.
[57] W. Shockley, *Bell Syst. Tech. J.* **1949**, *28*, 435.
[58] R. A. Street, M. Schoendorf, A. Roy, J. H. Lee, *Phys. Rev. B* **2010**, *81*, 205307.
[59] T. Kirchartz, B. E. Pieters, J. Kirkpatrick, U. Rau, J. Nelson, *Phys. Rev. B* **2011**, 83.
[60] S. R. Cowan, W. L. Leong, N. Banerji, G. Dennler, A. J. Heeger, *Adv. Funct. Mater.* **2011**, *21*, 3083.
[61] G. A. H. Wetzelaer, M. Kuik, M. Lenes, P. W. M. Blom, *Appl. Phys. Lett.* **2011**, *99*, 153506.
[62] Y. Sun, J. H. Seo, C. J. Takacs, J. Seifter, A. J. Heeger, *Adv. Mater.* **2011**, *23*, 1679.
[63] S. Zhang, L. Ye, W. Zhao, D. Liu, H. Yao, J. Hou, *Macromolecules* **2014**, *47*, 4653.
[64] J. Hofinger, C. Putz, F. Mayr, K. Gugujonovic, D. Wielend, M. C. Scharber, *Mater. Adv.* **2021**, *2*, 4291.

By providing the payment information below, you agree that you are responsible for the charges and taxes (as applicable), and that you will promptly pay the invoice in accordance with the terms thereof.

Please complete this form and return it via E-Mail to the Editorial Office:
Wiley-VCH GmbH Boschstraße 12, 69469 Weinheim
Germany
Tel.: (+49) 6201 606 235 or 432
Fax: (+49) 6201 606 500
Email: solar-rrl@wiley.com

Reprint Order Form

Manuscript No.: _____
Customer No.: (if available) _____
Purchase Order No.: _____ Author:

Charges for Reprints in Euro (excl. VAT), prices are subject to change. Minimum order 50 copies.

No. of pages	50 copies	100 copies	150 copies	200 copies	300 copies	500 copies
1– 4	345,—	395,—	425,—	445,—	548,—	752,—
5– 8	490,—	573,—	608,—	636,—	784,—	1077,—
9–12	640,—	739,—	786,—	824,—	1016,—	1396,—
13–16	780,—	900,—	958,—	1004,—	1237,—	1701,—
17–20	930,—	1070,—	1138,—	1196,—	1489,—	2022,—
every additional 4 pages	147,—	169,—	175,—	188,—	231,—	315,—

Information regarding VAT: The charges for publication of *cover pictures /reprints/issues/poster/Video abstracts/* are considered to be "supply of services" and therefore subject to German VAT. However, if you are an institutional customer outside Germany, the tax can be waived if you provide us with the valid VAT number of your company. Non-EU customers may have a VAT number starting with "EU" instead of their country code, if they are registered with the EU tax authorities. If you do not have a valid EU VAT number and you are a taxable person doing business in a non-EU country, please provide a certification from your local tax authorities confirming that you are a taxable person under local tax law. Please note that the certification must confirm that you are a taxable person and are conducting an economic activity in your country. **Note:** certifications confirming that you are a tax-exempt legal body (non-profit organization, public body, school, political party, etc.) in your country do not exempt you from paying German VAT.

Please bill me for

☐ no. of reprints

☐ high-resolution PDF file (330 Euro excl. VAT)
E-mail address: _____

❖ Special Offer:

If you order 200 or more reprints you will get a PDF file for half price.

Please note: It is not permitted to present the PDF file on the internet or on company homepages.

Cover Posters (prices excl. VAT)
Posters of published covers are available in two sizes:

☐ DIN A2 42 x 60 cm / 17 x 24in (one copy: 39 Euro)

☐ DIN A1 60 x 84 cm / 24 x 33in (one copy: 49 Euro)

Postage for shipping (prices excl. VAT)
overseas +25 Euro
within Europe +15 Euro

VAT number: _____

Mail reprints / copies of the issue to:

_____
_____
_____
_____
_____

Send bill to:

_____
_____
_____
_____

☐ **I will pay by bank transfer**

☐ **I will pay by credit card**

VISA, Mastercard and AMERICAN EXPRESS
For your security please use this link (Credit Card Token Generator) to create a secure code Credit Card Token and include this number in the form instead of the credit card data. Click here:
https://www.wiley-vch.de/editorial_production/index.php

CREDIT CARD TOKEN NUMBER

						V									

_____
Date, Signature

Wiley-VCH GmbH– A company of John Wiley & Sons, Inc. - Location of the Company: Weinheim - Trade Register: Mannheim, HRB 736569Managing Directors: Sabine Haag und Guido Herrmann

WILEY-VCH